A vast valley network beneath the Greenland Ice Sheet

Allison M. Chartrand[1,2]*, Joseph A. MacGregor[2], Mathieu Morlighem[3], Olga V. Sergienko[4], Helen Ockenden[5], William T. Colgan[6], Gong Cheng[3,7]

[1] Earth System Science Interdisciplinary Center, University of Maryland, College Park, Maryland, USA
[2] Cryospheric Sciences Laboratory, NASA Goddard Space Flight Center, Greenbelt, Maryland, USA
[3] Dept. of Earth Sciences, Dartmouth College, Hanover, New Hampshire, USA
[4] Program in Atmospheric and Oceanic Sciences, Princeton University, Princeton, New Jersey, USA
[5] L'Institut des Géosciences de l'Environnement, Université Grenoble-Alpes, France
[6] Geological Survey of Denmark and Greenland, Copenhagen, Denmark
[7] College of Surveying and Geo-informatics, Tongji University, Shanghai, China
* Corresponding author: J. A. MacGregor, joseph.a.macgregor@nasa.gov

Key Points

- Subglacial topography throughout Greenland's interior inferred using Ice Flow Perturbation Analysis can elucidate the island's history
- Contiguous subglacial valleys are widespread in Greenland and are usually connected to peripheral fjords
- The azimuths and junction angles of this subglacial valley network indicate it is modulated by tectonic inheritance and groundwater flow

Abstract

Mapping subglacial topography along the margin of the Greenland Ice Sheet was revolutionized by reconciling measurements of ice thickness and surface velocity using the principle of mass conservation. Despite evidence that many subglacial valleys resolved by that method extend upstream, it cannot be applied to the ice sheet's slower-flowing interior, where ice thickness observations are sparse. Here we apply Ice Flow Perturbation Analysis to surface elevation and velocity observations, revealing a vast, island-wide network of subglacial valleys connected to the peripheral valleys resolved by the mass conservation method. The morphology of this valley network further implicates Greenland's southern and eastern highlands as inception points for the ice sheet and also suggests that this network is modulated by both groundwater flow and Greenland's tectonic inheritance.

Plain Language Summary

The ice-free periphery of Kalaallit Nunaat (Greenland) hosts myriad landscapes dissected by valleys that typically trace back underneath its central ice sheet. A technique based on mass conservation has enabled us to better resolve the subglacial valleys near the edge of the ice sheet. However, inherent limitations to this technique still leave three quarters of the ice sheet with poorly resolved bedrock topography pockmarked by scores of disconnected holes. In this study, we use a method called Ice Flow Perturbation Analysis that takes advantage of observations of subtle bumps and troughs in the ice surface, which are typically due to larger variations in the underlying bedrock, to better reconstruct the bedrock topography beneath the ice sheet. Now, Greenland's bedrock topography includes many interconnected valleys that criss-cross the island beneath the ice sheet. Many of these valleys appear to originate from the southern and eastern highlands where the ice sheet is thought to have incepted. The regionally similar directions of many of these valleys suggest that past tectonic deformation within Greenland may have generated preferential pathways for them to form, and the pattern of angles at which the valleys meet suggests that groundwater flow influenced valley formation.

1. Introduction

Improving knowledge of subglacial topography beneath the Greenland and Antarctic ice sheets is crucial to interpret their current flow patterns and to project their futures (e.g., Aschwanden et al., 2016, 2019). Measuring this topography with airborne radar sounding has been a principal objective of many field campaigns (e.g., Holt et al., 2006; MacGregor et al., 2021; Robin et al., 1969). However, despite the synthesis of several decades of observations and the development of mass conservation (*MC*) techniques for more reliably infilling coastal regions by leveraging observations of surface velocity (Morlighem et al., 2011, 2017, 2025), observations remain sparse across the vast interiors of both ice sheets and substantial uncertainty in subglacial topography persists. For example, for the 150-m-resolution BedMachine Greenland (*BMG*) subglacial topography product, only 4.4% of its ice-sheet grid cells include a radar observation.

Presently, the subglacial topography of ice-sheet interiors or slower-flowing margins is unrealistically smooth compared to the periphery, while pockmarked along survey lines by sparsely sampled subglacial valleys. Accurately resolving these valleys is important, as ice flow and subglacial water drainage tend to focus toward them (e.g., Felikson et al., 2021; Joughin et al., 2013; MacKie et al., 2021; Morlighem et al., 2017). The planform morphology of these subglacial valleys and their associated networks also inform studies of landscape evolution beneath the ice sheet and its relation to long-term ice-sheet change (e.g., Jamieson et al., 2023; Paxman et al., 2021). The cross-sectional morphology of Greenland's subglacial valleys has been studied extensively by analyzing valley-intersecting radar surveys, rather than gridded subglacial topography products (e.g., Bamber et al., 2013; Paxman, 2023; Paxman et al., 2024). These studies revealed the pattern of fluvial and glacial incision across the island and its relation to the history of Greenland glaciation. However, because of the limitations in existing methods used to interpolate subglacial topography across the interior, it has not been possible to reliably study the island-wide planform morphology of Greenland's subglacial valley network (Cooper et al., 2016). Such analyses can clarify source regions and the climatic conditions under which they formed (e.g., Seybold et al., 2017).

It is well-established from theory and observations of subglacial topography and ice-surface elevation across both of Earth's ice sheets that significant perturbations in the bed can induce detectable variations on the surface (e.g., Chartrand et al., 2024; De Rydt et al., 2013; Ekholm et al., 1998; Gudmundsson, 2003, 2008; MacGregor et al., 2024; Paxman et al., 2021; Sergienko, 2012). Widespread observations of surface elevation and velocity are much more easily acquired than radar sounding data, motivating their use to indirectly constrain subglacial topography. To generate a more realistic landscape beneath parts of the interior of the Antarctic Ice Sheet for Bedmap3, Pritchard et al. (2025) guided interpolation of subglacial topography along radar-observed subglacial valleys using surface ice-flow streamlines. However, this streamline interpolation method cannot resolve the complex superposition of subglacial undulations (in either topography or basal slipperiness) across a range of wavelengths and azimuths that may give rise to a detectable surface expression (e.g., Ng et al., 2018; Ockenden et al., 2022; Sergienko, 2012), nor can it improve representation of subglacial topography within unsurveyed regions.

Recently, Ockenden et al. (2023, 2026) developed Ice Flow Perturbation Analysis (*IFPA*), a method that leverages bed-to-surface signal transfer theory from Gudmundsson (2003, 2008) and fine-resolution maps of surface elevation and velocity to better resolve interior Antarctic subglacial topography. Here we improve and apply this method to the Greenland Ice Sheet (*GrIS*), validate it against observations and compare it to the widely used BMG product. Focusing on newly resolved subglacial valleys, we consider the implications of this improved map of Greenland's subglacial topography for interpretation of its glaciological and geological history.

2. Data and Methods

2.1. Ice Flow Perturbation Analysis

We use a modified version of the IFPA algorithm described by Ockenden et al. (2023, 2026). IFPA uses linearized functions describing bed-to-surface transfer of ice-flow perturbations and weighted least-squares matrix inversion to estimate subglacial properties from Fourier transforms of ice surface elevation and velocity, which are IFPA's two primary data inputs. For surface elevation, we use the Making Earth System Data Records for Use in Research Environments (*MEaSUREs*) Greenland Ice Mapping Project (*GrIMP*) version 2 (*v2*) digital elevation model (*DEM*) (Howat et al., 2022) and then filter and resample it following MacGregor et al. (2024) onto the 150-m BMG grid. For surface velocity, we use the MEaSUREs Multi-year Greenland Ice Sheet Velocity Mosaic (Joughin et al., 2016, 2018). As for the surface DEM, we filter and resample the surface velocity to the BMG grid. **Text S1** and **Figures S1–S5** in **Supporting Information S1** provide additional details on IFPA.

IFPA requires a fixed domain (ice mask) and an initial estimate of ice thickness for its inversion, which we get from BMG v6 (Morlighem et al., 2025, 2026). We aim to improve representation of subglacial topography in the GrIS interior, where existing products have historically applied either ordinary kriging or streamline diffusion to interpolate between radar observations (Morlighem et al., 2017, 2025). Hence, we also use BMG's data source field, which distinguishes the interpolation method used, to combine IFPA with BMG and generate a *blended* subglacial topography.

We use ice-thickness data collected by the Center for Remote Sensing and Integrated Systems (*CReSIS*) and its predecessors during NASA airborne campaigns between 1993–2019 to evaluate IFPA and BMG performance (CReSIS, 2025). For comparison with gridded results, radar observations are binned onto the BMG grid and the median thickness is preserved. To identify regions where disrupted basal ice appears to perturb the surface, rather than subglacial relief (e.g., Cooper et al., 2019), we review the CReSIS radargrams and compare these results to a previous mapping of disrupted basal ice (Leysinger Vieli et al., 2018).

We improve the IFPA algorithm in three main ways. The first is our use of a thickness-dependent patch size, which substantially reduces IFPA differences from observations, better resolves small-scale variability in subglacial topography, and permits application near the GrIS margin where ice is thinner and where MC was not applied in BMG. Our second improvement concerns the mean slipperiness parameter ($\underline{C}$) across the GrIS. Although we mostly use a constant value $\underline{C}$ = 50, following Ockenden et al. (2026), we adjust it to be significantly higher (~1000) both near the ice-sheet edge and within the fast-flowing Northeast Greenland Ice Stream (*NEGIS*) using results from Sergienko et al. (2014).

Our third improvement involves the blending of IFPA-inferred subglacial topography with BMG. In contrast to Antarctica, there are no known megadune fields in Greenland to complicate interpretation of IFPA (Ockenden et al., 2026), and persistent features associated with surface processes (e.g., supraglacial lakes) are associated with the effects of basal conditions on ice flow (Sergienko, 2013). Further, because MC is predominantly used where GrIS surface mass balance is negative and crevasse fields are present (**Figure S3**), the blended topography is not significantly affected by potential complications in interpretation in those regions (Chudley et al., 2021; Fettweis, 2022). However, across four different region types, IFPA output is disfavored and BMG is preferred, so we weight them to generate a blended topography. We favor BMG over IFPA where: 1. MC is used by BMG, i.e., around faster-flowing outlet glaciers; 2. Disrupted basal ice is indicated by radargram inspection and oblong surface perturbations in the GrIMP flow-aware hillshade, which indicates flow-related perturbations in the ice surface (MacGregor et al., 2024); 3. Magnitudes of surface shear strain rates are high ($\geq 10^{-4}$ yr^{-1}), indicating a change in basal slipperiness; and 4. The abrupt change in surface-velocity azimuth across some sharper ice divides causes IFPA to malfunction. Finally, we correct for the residuals between the blended IFPA bed and radar observations following Ockenden et al. (2026).

2.2. Manual and automated feature mapping

We apply two separate methods to map features in the blended subglacial topography. First, we manually trace the centerline of subglacial valleys in the IFPA subglacial topography at a scale of 1:750,000, focusing on those that are ≥10 km long and ≥1 km wide, i.e., the same criteria as MacGregor et al. (2024). We record where these valleys are also apparent in BMG and if they connect to peripheral valleys. Second, to independently evaluate the dominant azimuths of major features in the IFPA subglacial topography, whether they are subglacial valleys or not, we use Hough transforms. We divide the GrIS into 75-km squares; for each square, we generate 12 distinct unidirectional hillshades at 15° illumination-azimuth intervals. For each hillshade, we use Canny edge detection to identify dominant features and record the 100 most prominent azimuth/offset peaks in the Hough transform of the resulting binary image. **Text S2** in **Supporting Information S1** provides additional details.

2.3. Valley network morphology

We analyze Greenland's valley network morphology using the blended topography after correcting for its total isostatic response to unloading of the GrIS (Paxman et al., 2022, 2026). This choice assumes implicitly that the planform structure of this valley network is due primarily to glaciofluvial erosion either prior to or during the inception of the GrIS, rather than subsequent subglacial erosion during the Pleistocene. We use TopoToolbox to map the rebounded valley network automatically (Schwangart & Scherler, 2014). Branching angles of stream networks – distinct from their azimuths – provide information about the climate in which the networks formed. We modify TopoToolbox to measure the branching angle of all network intersections following Seybold et al. (2017). For this analysis and all maps shown, we use the NSIDC Sea Ice Polar

Stereographic North projection (EPSG:3413), which is conformable and hence angle-preserving. **Text S3** in Supporting Information S1 provides additional details.

3. Results

We test our improvements to IFPA at the onset of Ryder Glacier in northern Greenland (Figures 1A, S2). Adjusting the patch size based on the mean ice thickness significantly decreases the root mean square error (*RMSE*) between IFPA and radar observations from 93 to 65 m. Because of these smaller patch sizes and because most of the GrIS is land-terminating, we can apply IFPA toward the edge of most of the ice sheet, including where MC is not applied (Figure 2B). Separately, while optimizing $\underline{C}$ for each patch yields the lowest RMSE (56 m), the resulting topography is less geomorphologically coherent relative to when a uniform $\underline{C}$ is used. Our choice of a uniform $\underline{C}$ value (50) produces perturbations consistent with radar observations and yields an acceptable RMSE (65 m) that is close to that of BMG (55 m).

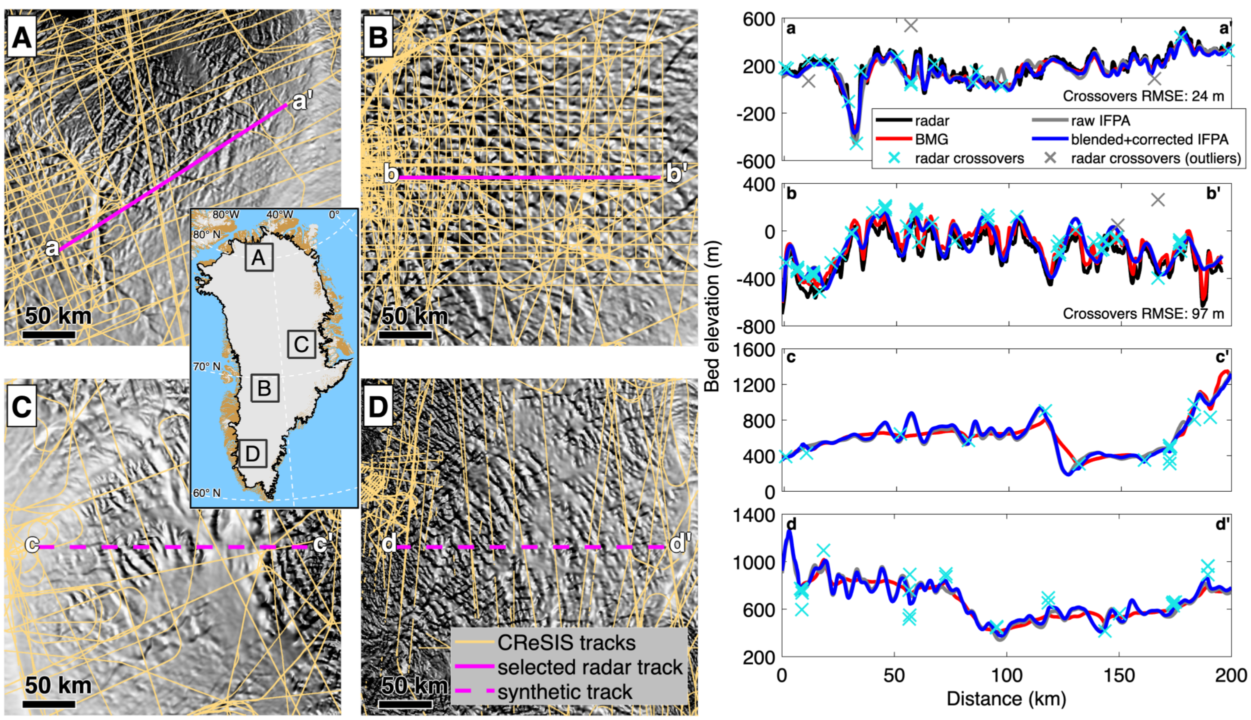

Figure 1.
GrIMP flow-aware hillshade for four 250-km-square regions across the GrIS (MacGregor et al., 2024). (A) and (B) show 200-km portions of two existing survey lines (20080716_02, 20120503_03), whereas (C) and (D) show two synthetic cross-sections that have *not* been surveyed. Profiles on right show radar-observed subglacial topography, BMG, raw IFPA (uncorrected), blended and radar-corrected IFPA, and crossovers from intersecting radar surveys. The radar correction to IFPA is generally small (18 ± 27 m). Crossovers with differences greater than the standard deviation of the detrended profile are considered outliers and not included in crossover RMSEs.

The surface DEM used by BMG (GrIMP v1; Howat et al., 2017) contains more artifacts than GrIMP v2, which we use for the IFPA inversion. However, we use a plane-fit of GrIMP v1 for each patch to re-dimensionalize IFPA outputs, which enables direct comparison of IFPA and BMG. We compare the RMSE of BMG and IFPA ice thicknesses with CReSIS radar data where those data are the primary source of observations. For those parts of the GrIS, the blended, radar-corrected topography performs significantly better (84 m) than both the raw IFPA-inferred topography (110 m) and BMG (90 m). Notably, the highest RMSE values for both BMG (125 m) and raw IFPA (156 m) are found where the blended topography uses BMG exclusively (**Figure 2B**). Those problematic regions are also where the standard deviations of IFPA for overlapping patches are typically the highest and where we expect its underlying assumptions to break down (Ockenden et al., 2026). In the MC regions where IFPA and BMG are weighted together, RMSE increases slightly (from 63 m to 66 m), although the blending in these regions reduces some MC artifacts. The blended topography significantly improves accuracy everywhere else, especially where it exclusively uses IFPA (from 73 to 61 m). **Figures S6–S9** in **Supporting Information S1** compare IFPA and BMG and their error estimates. All following discussion of IFPA refers to the radar-corrected, blended topography.

Application of IFPA to Greenland reveals detailed subglacial topography at scales of ~2–30 km that is consistent with BMG in densely surveyed regions but diverges in sparsely surveyed regions (**Figure 1**), especially in terms of the density and continuity of major subglacial valleys (>2 km wide). IFPA reproduces the variability in both the subglacial topography along survey lines and at available crossovers along synthetic cross-sections. Crucially, both IFPA and BMG subglacial topography align with relief visible in the flow-aware hillshade along existing survey lines, but only IFPA reproduces similar relief elsewhere. Particularly along the synthetic cross-section in southern Greenland (**Figure 1D**), crossover errors are larger, indicating steep and rough terrain that is more fully captured by IFPA.

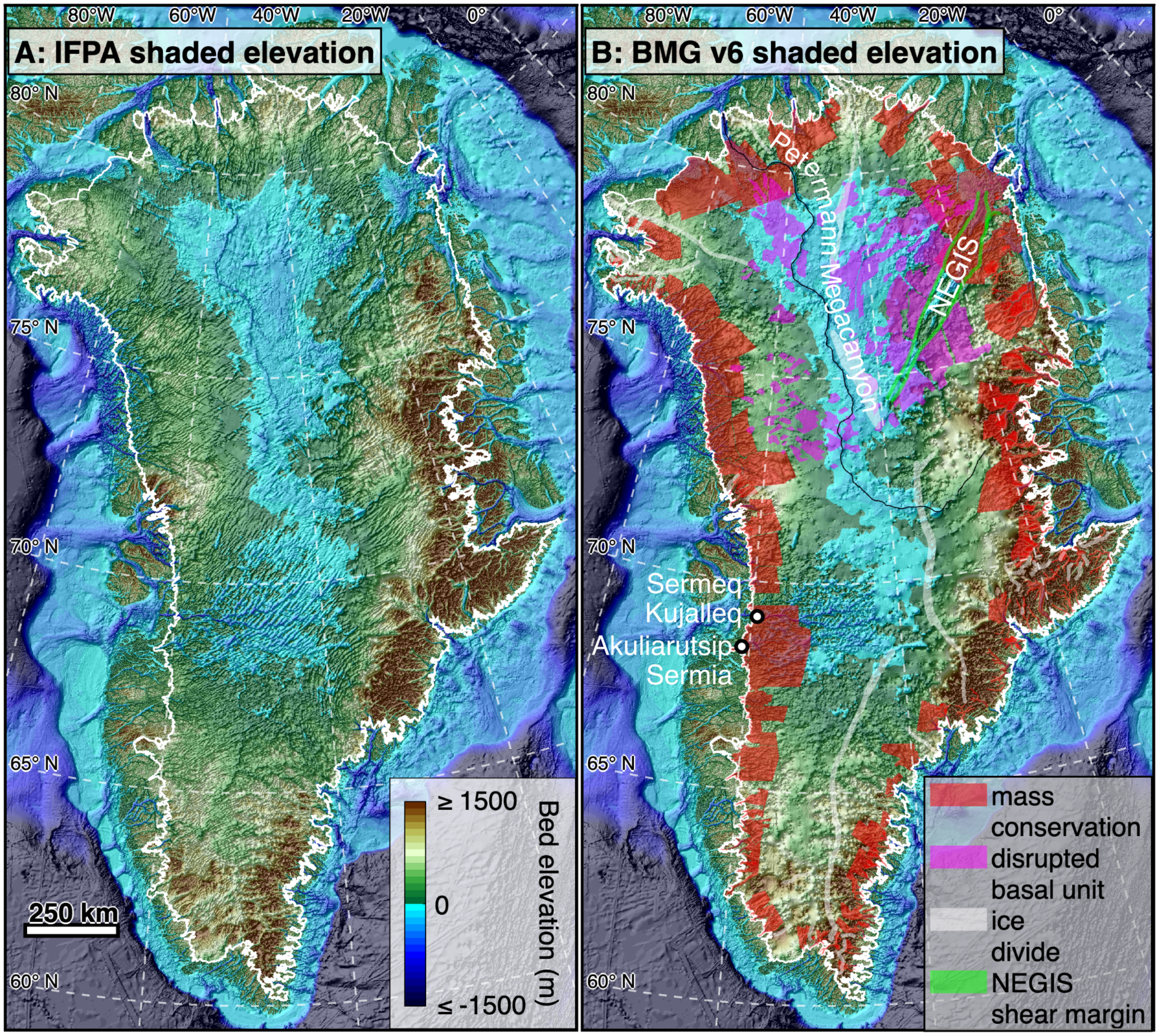

Figure 2.
(A) Colorized hillshade of blended (IFPA + BMG) subglacial topography for Greenland, with illumination from the southeast (135º) at 45º elevation. White line is GrIS terminus. (B) Same as (A) but for BMG. Highlighted regions are where BMG is used primarily or exclusively. Key locations mentioned in text are labeled.

We next compare hillshades of IFPA and BMG subglacial topography (Figure 2). For the synthetic cross-sections, IFPA predicts greater subglacial relief than BMG across the ice-sheet interior, whereas BMG is smoother except along survey lines. The relief in IFPA more closely aligns with both that within ice-free regions and the flow-aware hillshade on-ice. IFPA shows that many of the subglacial valleys resolved by MC along the ice-sheet periphery extend much farther into the interior – sometimes hundreds of kilometers more than in BMG. We manually map 1943 subglacial valleys beneath the GrIS, of which 34% are identified by IFPA and are not present in BMG (Figure 3A), and 52% of those visible in BMG are extended farther by IFPA. Subglacial valleys confine the flow of nearly all of the GrIS's 239 largest outlet glaciers (terminus ≥1.5 km wide; Joughin et al., 2021), and most (~70%) of these are extended farther upstream in our blended subglacial topography; most that are not extended are in the SE drainage basin and are relatively small (discharge <1 Gt yr^{-1}). Our improved mapping of subglacial valleys is most apparent in the CW, NO and CE drainage basins. Based on mapped valley presence in a 10-km grid, the areal extent of this valley network is nearly doubled in the blended subglacial topography (74% of the GrIS) as compared to BMG (39%). This extent is limited primarily by where the blended subglacial topography does not use IFPA, mostly due to disrupted basal units within the northern GrIS (**Figure 2B**).

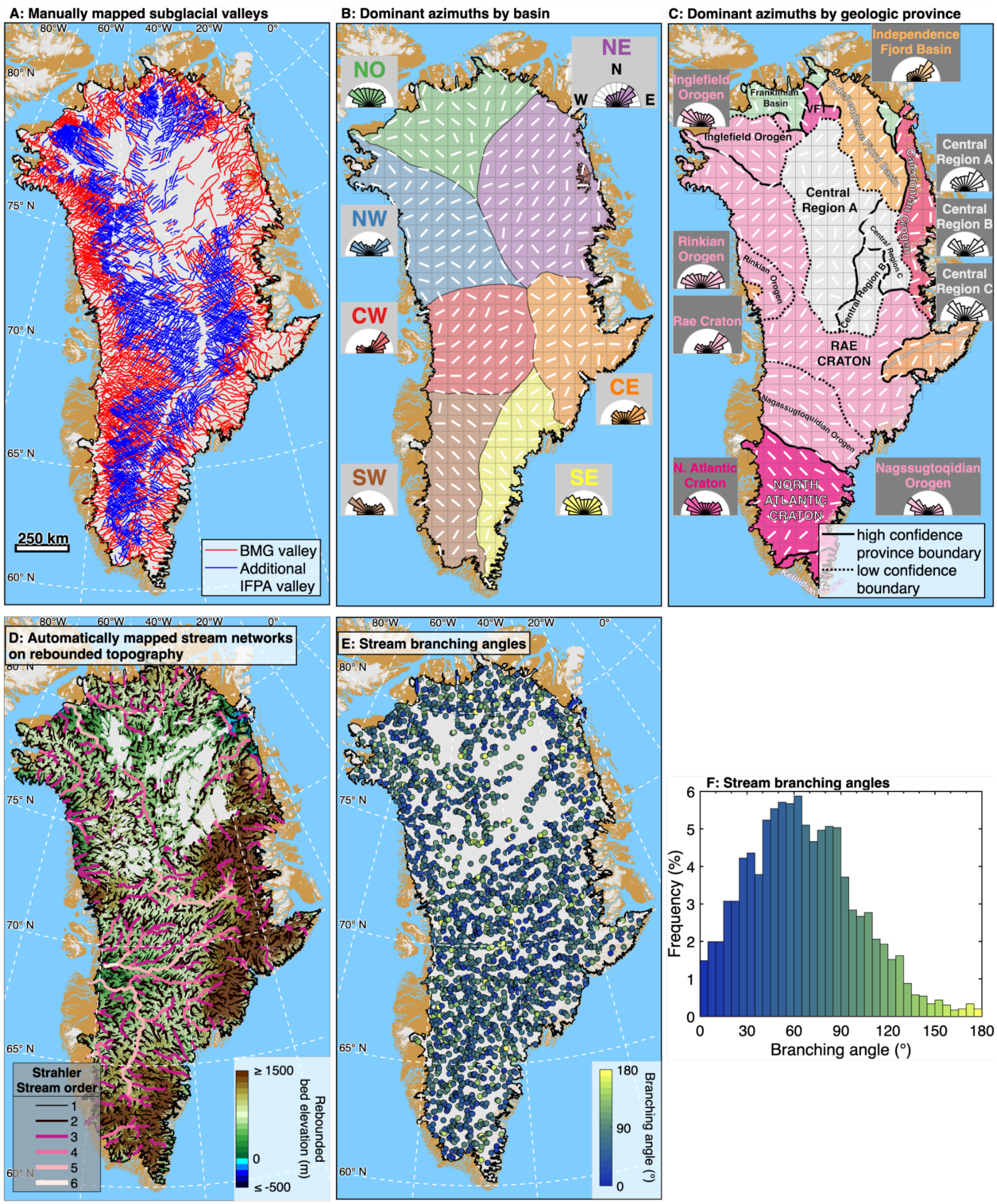

Figure 3.
(A) Manually mapped subglacial valleys across the GrIS. (B) Dominant azimuth of major subglacial topographic lineations within 75-km squares; polar histograms show the azimuthal distribution of lineations within each ice-drainage basin (Mouginot et al., 2019). (C) Same as (B) but for major geologic provinces (MacGregor et al., 2024). (D) Automatically mapped valley

network in rebounded topography; network segments are colored by Strahler stream order. Grayed-out regions in northern Greenland are where disrupted basal units prevented application of IFPA and are ignored in this analysis. (E, F) Branching angles between intersecting automatically mapped valleys.

Our azimuthal analysis reveals distinct patterns in valley orientation (**Figure 3B**), with a typically bimodal distribution of azimuths by drainage basin, with southwest–northeast being most common (CW, NW, NE, and CE drainage basins) and southeast–northwest next most common (SW, NO, and SE). These patterns confirm and accentuate those inferred from the flow-aware hillshade by MacGregor et al. (2024), and they are also qualitatively consistent with our manually mapped subglacial valleys but bear no clear relation to modern ice-flow azimuths (**Figure S10B**). The same azimuthal analysis of BMG yields only weakly bimodal distributions within the NW and NO basins (**Figure S10C**). Finally, we also identify distinct azimuthal distributions between apparent subglacial geologic provinces (**Figure 3C**), especially between the Nagssugtoqidian Orogen and the southern Rae Craton, and between the Rinkian Orogen and the northwestern Rae Craton. These distinctions further support their delineations by MacGregor et al. (2024).

Automatic mapping of the valley network in the rebounded topography produces a similar network to that which we mapped manually, but which is more extensive and interconnected as the algorithm follows more subtle topographic gradients than we can map visually (**Figure 3A, D**). Several (22) larger (>10,000 km^2) dendritic basins are outlined, although the limitations of our blended topography are also apparent, as many basins in northern Greenland – particularly those connected to the Petermann Megacanyon (Paxman et al., 2021) – terminate prematurely near ice divides or disrupted basal units. In southern Greenland (<68ºN), these basins coalesce around Greenland's southern highlands, whereas most basins farther north coalesce toward the eastern highlands, including one of the two largest basins that terminates at Sermeq Kujalleq (Jakobshavn Isbræ) in central western Greenland. Our stream network contrasts with that of Cooper et al. (2016), as we find that the southern highlands are not also a source region for Sermeq Kujalleq, but instead for Akuliarutsip Sermia, ~100 km to its southwest.

Previous studies of subaerial river networks analyzed the mean branching angle from each individual basin to determine their climatic relationships. However, here we report on and analyze 3031 branching angles for the GrIS subglacial valley network as a whole because of the above-mentioned limitations in basin delineation and the smaller total area we consider, i.e., the GrIS is only 21% the size of the contiguous United States investigated by Seybold et al. (2017). These branching angles do not evince any obvious spatial pattern, either across Greenland or within individual basins, but their distribution peaks between ~50–65º (**Figure 3E,F**). This low-to-intermediate peak range is diagnostic of climates where groundwater flow or soil erosion are non-negligible but smaller contributors to channel incision than precipitation or surface runoff (Seybold et al., 2017, 2018).

4. Discussion

4.1. IFPA methodology

A key advantage of IFPA over the streamline diffusion method presently used by BMG for the GrIS interior is that IFPA produces an estimate of the variability in subglacial topography that is constrained by fine-resolution surface observations and bed-to-surface transfer theory. IFPA-inferred subglacial topography in Greenland better reflects ice-surface variability where radar observations are not available, and the radar correction and blending improves accuracy relative to BMG and ensures that IFPA output is not preserved where we expect it to be unreliable *a priori*. Hence, IFPA is part of a growing suite of methods for inferring subglacial topography with greater fidelity to other relevant ancillary remote-sensing observations while maintaining fidelity to radar observations, with the overall goal of generating more credible maps of subglacial topography (e.g., Cheng et al., 2024; Maffezzoli et al., 2025). Given the limitations of IFPA in resolving subglacial topography beneath some parts of the GrIS, particularly beneath disrupted basal units, we highlight these regions as potential foci for future airborne radar surveys or other methods (**Figure 2B**).

IFPA requires an estimate of slipperiness to infer subglacial topography. Like Ockenden et al. (2026), we use a uniform slipperiness value for most of the ice sheet, which is unlikely to be an accurate representation of the subglacial conditions. However, an advantage of IFPA is that when using a uniform slipperiness value, varying this value only changes the amplitude of the perturbations, so we are confident in the locations of inferred subglacial valleys if not their absolute relief (**Figure S2**; Ockenden et al., 2023). Most of the large valleys we identified are coincident with prominent surface lineations traced in the GrIMP flow-aware hillshade by MacGregor et al. (2024) (**Figure 3A**), increasing confidence in their previous interpretation that those lineations are subglacial valleys.

4.2. Subglacial geology and geomorphology

Patterns in the texture and dominant azimuth of subglacial topography revealed by IFPA provide new context for interpretations of the geologic and geomorphic history of Greenland. Our analyses are consistent with the hypothesis that alpine-style subglacial geomorphology dominates the region southeast of NEGIS and adjacent to the Greenland eastern highlands and has likely been preserved since at least the Pliocene (Bierman et al., 2016; MacGregor et al., 2024; Paxman et al., 2024). Where BMG only hints at substantial topographic relief, IFPA reveals a subglacial mountain range with an interconnected valley network similar to that inferred by Paxman et al. (2024) both along *and* between radar surveys, with increasingly greater relief to the east (**Figure 2**). This valley network spans the transition from a likely frozen bed to the south and a likely thawed bed to the north, closer to NEGIS (MacGregor et al., 2022). IFPA also better resolves several deeply incised subglacial valleys that slope approximately radially inland from this region, suggesting preferential pathways for past subglacial or glaciofluvial erosion beneath what is now slow-moving and likely cold-based ice with little erosive potential.

Based on their subaerial exposures, distinct geologic provinces beneath the GrIS may be partly distinguishable by their subglacial topography (MacGregor et al., 2024). The clearest example thereof is in far southern Greenland, another region hypothesized to have remained ice-covered or minimally eroded since the late Pliocene (Paxman et al., 2024), where IFPA also generates rough subglacial topography, and which is an apparent source region for several valley networks (**Figure 3D**). There, ice is presumed to be warmer and firn aquifers are more common, limiting the success of radar sounding and resulting in an unnaturally smooth BMG, in contrast with the steep mountains that fringe the southernmost GrIS. With IFPA, these subglacial southern highlands are revealed to possess similar relief to coastal regions, and this relief extends north into a subglacial valley network that is less clearly visible in either the surface or BMG (**Figures 1D**, **2**). Notably, part of the subglacial valley network we identify as draining those southern highlands is nearly coincident with the northern boundary of the North Atlantic Craton inferred by MacGregor et al. (2024), although the azimuthal distribution in the North Atlantic Craton is similar to that in the Nagssugtoqidian Orogen to the north (**Figure 3C**). We also identify a valley network along the northwestern subglacial boundary of the Nagssugtoqidian Orogen, suggesting a difference between the erosivity of that orogen and the Rae Craton farther north, and consistent with their apparent difference in azimuthal distribution.

The dominant southwest–northeast azimuth of the subglacial valley network, which is most apparent in the CW, NW, NE and CE drainage basins (**Figure 3B**), is striking and indicates an underlying geologic influence, based on studies of valley networks in deglaciated terrain (Mudd et al., 2022). This particular azimuth is reminiscent of the left-lateral shear pattern proposed by Beh (1975). They hypothesized that the Greenland plate deformed between the Late Cretaceous and Middle Eocene to accommodate sea-floor spreading in Baffin Bay and the Labrador Sea. This shearing was hypothesized to be accompanied by strike–slip motion along the so-called "Wegener Fault" in Nares Strait between Ellesmere Island and Greenland. This two-part hypothesis was soon discarded once sufficient geological and structural observations convincingly precluded the existence of the Wegener Fault (Rasmussen & Dawes, 2011; Srivastava & Falconer, 1982). However, it remains possible that parts of Greenland's plate experienced post-Late Cretaceous shear, and that this tectonic inheritance has been subsequently exploited during valley incision (MacGregor et al., 2024). Critically, GNSS stations across Greenland record differences in horizontal plate motion directions that are presently unresolved (Berg et al., 2025), potentially indicating that the Greenland plate is subtly shearing presently, albeit in a roughly orthogonal direction (northwest–southeast) to that proposed by Beh (1975). The combination of these modern observations and the azimuthal bias of the vast valley network we resolve suggests that the hypothesis of a rigid Greenland plate, which is predominant in reconstructions of past plate tectonics (e.g., Merdith et al., 2021), should be reconsidered.

Our analysis of GrIS subglacial valley branching angles is the first to infer Greenlandic paleoclimatic conditions in this manner, so our interpretation proceeds cautiously. At least two regions that were formerly more extensively glaciated have been investigated (Alaska and Mars; Seybold et al., 2018), yielding contrasting but nevertheless informative results (high and low mean branching angles and aridity indices, respectively). A modal branching angle between 50–65º beneath the GrIS suggests that an aridity index (ratio of precipitation to potential evapotranspiration) of ~0.1–1 was predominant during valley incision. This implies that the process of landscape channelization there includes greater contributions from overland flow than the combination of diffusive groundwater flow and soil erosion, but also that the latter combination is non-negligible (Seybold et al., 2018). The influence of groundwater flow appears consistent with recent Greenland subglacial groundwater observations and modeling, some of which indicate the acute sensitivity of this system to changing ice-sheet loading (e.g., Bessette et al., 2021; Liljedahl et al., 2021; Robel et al., 2023). While not directly indicative of the modern presence of a widespread and dynamic groundwater system beneath the GrIS, our branching analysis suggests that such a system has had a long-term influence on the geomorphic evolution of Greenland.

5. Conclusions

With an improved algorithmic implementation, application of IFPA to the GrIS reveals striking new detail in its subglacial topography. As for earlier implementations of IFPA in Antarctica, we generate a subglacial topography with greater physical consistency with subaerial observations than BMG while improving fidelity to radar surveys. IFPA connects hundreds of subglacial valleys across the GrIS interior that were previously either discontinuous or absent in BMG, provides additional support for recent interpretations of the geologic history of Greenland, and offers new insight into the controls on the geomorphic evolution of the island. Our blended map expands the regions where the subglacial topography is based on an interpolation that is more consistent with the physics of ice flow – from just the MC regions along the ice-sheet periphery in BMG to now most of the GrIS. This new map resolves finer details in subglacial topography that will ultimately improve our ability to model the evolution of the GrIS.

Open Research

All new datasets generated by this study and associated code are openly archived (Chartrand et al., 2026; Chartrand, 2026).

Acknowledgments

NASA's Earth Surface and Interior Program supported AMC, JAM, MM and OS. WC is supported by the Novo Nordisk Foundation (NNF23OC00807040). We thank the GrIMP and QGreenland projects, the NASA MEaSUREs program, the NSIDC, the NSF Arctic Data Center, the GEUS Dataverse and Zenodo for archiving and distribution of many of the datasets used in this study. We thank Lauren C. Andrews, Jonathan L. Bamber, Thomas R. Chudley, Michael A. Cooper, Denis Felikson, Aslak Grinsted and Mansa Krishna for valuable discussions. We thank the Editor Christine F. Dow, Guy J.G. Paxman and an anonymous referee for valuable feedback.

Conflict of Interest Statement

The authors have no conflicts of interest to disclose.

Author Contributions

Conceptualization: Allison M. Chartrand, Joseph A. MacGregor, William T. Colgan, Mathieu Morlighem, Olga Sergienko; Data curation: Allison Chartrand, Joseph A. MacGregor, Mathieu Morlighem; Formal analysis: Allison M. Chartrand; Funding acquisition: Joseph A. MacGregor, Mathieu Morlighem, Olga Sergienko; Investigation: Allison M. Chartrand, Joseph A. MacGregor, Mathieu Morlighem, Olga V. Sergienko, Helen Ockenden, William T. Colgan, Gong Cheng; Methodology: Allison M. Chartrand, Joseph A. MacGregor, Helen Ockenden; Project

Administration: Joseph A. MacGregor; Software: Allison M. Chartrand, Joseph A. MacGregor, Helen Ockenden; Validation: Allison M. Chartrand, Joseph A. MacGregor, Mathieu Morglihem, Olga Sergienko; Visualization: Allison M. Chartrand, Joseph A. MacGregor; Writing – original draft: Allison M. Chartrand, Joseph A. MacGregor; Writing – review & editing: Allison M. Chartrand, Joseph A. MacGregor, Mathieu Morlighem, Olga V. Sergienko, Helen Ockenden, William T. Colgan, Gong Cheng

References

Andrews, L. C., Catania, G. A., Hoffman, M. J., Gulley, J. D., Lüthi, M. P., Ryser, C., et al. (2014). Direct observations of evolving subglacial drainage beneath the Greenland Ice Sheet. *Nature*, *514*(7520), 80–83. https://doi.org/10.1038/nature13796

Aschwanden, A., Fahnestock, M. A., & Truffer, M. (2016). Complex Greenland outlet glacier flow captured. *Nature Communications*, *7*(1), 10524. https://doi.org/10.1038/ncomms10524

Aschwanden, A., Fahnestock, M. A., Truffer, M., Brinkerhoff, D. J., Hock, R., Khroulev, C., et al. (2019). Contribution of the Greenland Ice Sheet to sea level over the next millennium. *Science Advances*, *5*(6), eaav9396. https://doi.org/10.1126/sciadv.aav9396

Bamber, J. L., Siegert, M. J., Griggs, J. A., Marshall, S. J., & Spada, G. (2013). Paleofluvial Mega-Canyon Beneath the Central Greenland Ice Sheet. *Science*, *341*(6149), 997–999. https://doi.org/10.1126/science.1239794

Beh, R. (1975). Evolution and geology of Western Baffin Bay and Davis Strait, Canada. In *Canada's Continental Margins and Offshore Petroleum Exploration, Memoir 4* (pp. 453–476). Calgary, Alberta, Canada: Canadian Society of Petroleum Geologists.

Berg, D. L., Adhikari, S., Hassan, J., Steffen, R., Steffen, H., Willis, M., & Khan, S. A. (2025). Estimation and Attribution of Horizontal Land Motion Measured by the Greenland GNSS Network. *Journal of Geophysical Research: Solid Earth*, *130*(9), e2024JB030847. https://doi.org/10.1029/2024JB030847

Bessette, J. T., Schroeder, D. M., Jordan, T. M., & MacGregor, J. A. (2021). Radar-Sounding Characterization of the Subglacial Groundwater Table Beneath Hiawatha Glacier, Greenland. *Geophysical Research Letters*, *48*(10), e2020GL091432. https://doi.org/10.1029/2020GL091432

Bierman, P. R., Shakun, J. D., Corbett, L. B., Zimmerman, S. R., & Rood, D. H. (2016). A persistent and dynamic East Greenland Ice Sheet over the past 7.5 million years. *Nature*, *540*(7632), 256–260. https://doi.org/10.1038/nature20147

Chartrand, A.M. (2026). AllisonCh/Greenland_IFPA: Greenland_IFPA publication release (v1.0.2). [Software]. Zenodo. https://doi.org/10.5281/zenodo.20651289

Chartrand, A. M., Howat, I. M., Joughin, I. R., & Smith, B. E. (2024). Thwaites Glacier thins and retreats fastest where ice-shelf channels intersect its grounding zone. *The Cryosphere*, *18*(11), 4971–4992. https://doi.org/10.5194/tc-18-4971-2024

Chartrand, A. M., MacGregor, J. A., Morlighem, M., Sergienko, O. V., Ockenden, H., Colgan, W. T., & Cheng, G. (2026). Datasets accompanying manuscript: A vast valley network beneath the Greenland Ice Sheet (Version 1) [Data set]. Zenodo. https://doi.org/10.5281/zenodo.18245711

Cheng, G., Morlighem, M., & Francis, S. (2024). Forward and Inverse Modeling of Ice Sheet Flow Using Physics-Informed Neural Networks: Application to Helheim Glacier, Greenland. *Journal of Geophysical Research: Machine Learning and Computation*, *1*(3), e2024JH000169. https://doi.org/10.1029/2024JH000169

Chu, W., Creyts, T. T., & Bell, R. E. (2016). Rerouting of subglacial water flow between neighboring glaciers in West Greenland. *Journal of Geophysical Research: Earth Surface*, *121*(5), 925–938. https://doi.org/10.1002/2015JF003705

Chudley, T. R., Christoffersen, P., Doyle, S. H., Dowling, T. P. F., Law, R., Schoonman, C. M., et al. (2021). Controls on Water Storage and Drainage in Crevasses on the Greenland Ice Sheet. *Journal of Geophysical Research: Earth Surface*, *126*(9), e2021JF006287. https://doi.org/10.1029/2021JF006287

Colgan, W., MacGregor, J. A., Mankoff, K. D., Haagenson, R., Rajaram, H., Martos, Y. M., et al. (2021). Topographic Correction of Geothermal Heat Flux in Greenland and Antarctica. *Journal of Geophysical Research: Earth Surface*, *126*(2), e2020JF005598. https://doi.org/10.1029/2020JF005598

Cooper, M. A., Michaelides, K., Siegert, M. J., & Bamber, J. L. (2016). Paleofluvial landscape inheritance for Jakobshavn Isbræ catchment, Greenland. *Geophysical Research Letters*, *43*(12), 6350–6357. https://doi.org/10.1002/2016GL069458

Cooper, M. A., Jordan, T. M., Siegert, M. J., & Bamber, J. L. (2019). Surface Expression of Basal and Englacial Features, Properties, and Processes of the Greenland Ice Sheet. *Geophysical Research Letters*, *46*(2), 783–793. https://doi.org/10.1029/2018GL080620

CReSIS. (2025). L2 Ice Thickness, Ice Surface, and Ice Bottom elevations [Data set]. Digital Media, Lawrence, Kansas, USA. Retrieved from http://data.cresis.ku.edu/

De Rydt, J., Gudmundsson, G. H., Corr, H. F. J., & Christoffersen, P. (2013). Surface undulations of Antarctic ice streams tightly controlled by bedrock topography. *The Cryosphere*, *7*(2), 407–417. https://doi.org/10.5194/tc-7-407-2013

Ehrenfeucht, S., Dow, C., McArthur, K., Morlighem, M., & McCormack, F. S. (2025). Antarctic Wide Subglacial Hydrology Modeling. *Geophysical Research Letters*, *52*(1), e2024GL111386. https://doi.org/10.1029/2024GL111386

Ekholm, S., Keller, K., Bamber, J. L., & Gogineni, S. P. (1998). Unusual surface morphology from digital elevation models of the Greenland Ice Sheet. *Geophysical Research Letters*, *25*(19), 3623–3626. https://doi.org/10.1029/98GL02589

Felikson, D., A. Catania, G., Bartholomaus, T. C., Morlighem, M., & Noël, B. P. Y. (2021). Steep Glacier Bed Knickpoints Mitigate Inland Thinning in Greenland. *Geophysical Research Letters*, *48*(2), e2020GL090112. https://doi.org/10.1029/2020GL090112

Fettweis, X. (2022). Modèle Atmosphérique Régional (MAR) version 3.11 regional climate model output, 1979-2019, Greenland domain, 10 kilometer (km) horizontal resolution [Data set]. urn:node:ARCTIC. https://doi.org/10.18739/A28G8FJ7F

Gudmundsson, G. H. (2003). Transmission of basal variability to a glacier surface. *Journal of Geophysical Research: Solid Earth*, *108*(B5). https://doi.org/10.1029/2002JB002107

Gudmundsson, G. H. (2008). Analytical solutions for the surface response to small amplitude perturbations in boundary data in the shallow-ice-stream approximation. *The Cryosphere*, *2*(2), 77–93. https://doi.org/10.5194/tc-2-77-2008

Haran, T., Bohlander, J., Scambos, T., Painter, T., & Fahnestock, M. (2013). MEaSUREs MODIS Mosaic of Greenland 2005 (MOG2005) Image Map, Version 1. *NASA National Snow and Ice Data Center Distributed Active Archive Center (DAAC) Data Set*, IAGYM8Q26QRE. https://doi.org/10.5067/IAGYM8Q26QRE

Holt, J. W., Peters, M. E., Kempf, S. D., Morse, D. L., & Blankenship, D. D. (2006). Echo source discrimination in single-pass airborne radar sounding data from the Dry Valleys, Antarctica: Implications for orbital sounding of Mars. *Journal of Geophysical Research: Planets*, *111*(E6). https://doi.org/10.1029/2005JE002525

Howat, I., Negrete, A., & Smith, B. (2017). MEaSUREs Greenland Ice Mapping Project (GIMP) Digital Elevation Model from GeoEye and WorldView Imagery, Version 1 [Data set]. NASA National Snow and Ice Data Center Distributed Active Archive Center. https://doi.org/10.5067/H0KUYVF53Q8M

Howat, I., Negrete, A., & Smith, B. (2022). MEaSUREs Greenland Ice Mapping Project (GrIMP) Digital Elevation Model from GeoEye and WorldView Imagery, Version 2 [Data set]. NASA National Snow and Ice Data Center Distributed Active Archive Center. https://doi.org/10.5067/BHS4S5GAMFVY

Jamieson, S. S. R., Ross, N., Paxman, G. J. G., Clubb, F. J., Young, D. A., Yan, S., et al. (2023). An ancient river landscape preserved beneath the East Antarctic Ice Sheet. *Nature Communications*, *14*(1), 6507. https://doi.org/10.1038/s41467-023-42152-2

Joughin, I., Das, S. B., Flowers, G. E., Behn, M. D., Alley, R. B., King, M. A., et al. (2013). Influence of ice-sheet geometry and supraglacial lakes on seasonal ice-flow variability. *The Cryosphere*, *7*(4), 1185–1192. https://doi.org/10.5194/tc-7-1185-2013

Joughin, I., Smith, B., Howat, I., & Scambos, T. (2016). MEaSUREs Multi-year Greenland Ice Sheet Velocity Mosaic, Version 1 [Data set]. NASA National Snow and Ice Data Center Distributed Active Archive Center. https://doi.org/10.5067/QUA5Q9SVMSJG

Joughin, I., Smith, B. E., & Howat, I. M. (2018). A complete map of Greenland ice velocity derived from satellite data collected over 20 years. *Journal of Glaciology*, *64*(243), 1–11. https://doi.org/10.1017/jog.2017.73

Joughin, I., Moon, T., Joughin, J., & Black, T. (2021). MEaSUREs Annual Greenland Outlet Glacier Terminus Positions from SAR Mosaics, Version 2 [Data set]. NASA National Snow and Ice Data Center Distributed Active Archive Center. https://doi.org/10.5067/ESFWE11AVFKW

Leysinger Vieli, G. J.-M. C., Martín, C., Hindmarsh, R. C. A., & Lüthi, M. P. (2018). Basal freeze-on generates complex ice-sheet stratigraphy. *Nature Communications*, *9*(1), 4669. https://doi.org/10.1038/s41467-018-07083-3

Liljedahl, L. C., Meierbachtol, T., Harper, J., van As, D., Näslund, J.-O., Selroos, J.-O., et al. (2021). Rapid and sensitive response of Greenland's groundwater system to ice sheet change. *Nature Geoscience*, 1–5. https://doi.org/10.1038/s41561-021-00813-1

MacGregor, J. A., Studinger, M., Arnold, E., Leuschen, C. J., Rodríguez-Morales, F., & Paden, J. D. (2021). Brief communication: An empirical relation between center frequency and measured thickness for radar sounding of temperate glaciers. *The Cryosphere*, *15*(6), 2569–2574. https://doi.org/10.5194/tc-15-2569-2021

MacGregor, J. A., Chu, W., Colgan, W. T., Fahnestock, M. A., Felikson, D., Karlsson, N. B., et al. (2022). GBaTSv2: a revised synthesis of the likely basal thermal state of the Greenland Ice Sheet. *The Cryosphere*, *16*(8), 3033–3049. https://doi.org/10.5194/tc-16-3033-2022

MacGregor, J. A., Colgan, W. T., Paxman, G. J. G., Tinto, K. J., Csathó, B., Darbyshire, F. A., et al. (2024). Geologic Provinces Beneath the Greenland Ice Sheet Constrained by Geophysical Data Synthesis. *Geophysical Research Letters*, *51*(8), e2023GL107357. https://doi.org/10.1029/2023GL107357

MacKie, E. J., Schroeder, D. M., Zuo, C., Yin, Z., & Caers, J. (2021). Stochastic modeling of subglacial topography exposes uncertainty in water routing at Jakobshavn Glacier. *Journal of Glaciology*, *67*(261), 75–83. https://doi.org/10.1017/jog.2020.84

Maffezzoli, N., Rignot, E., Barbante, C., Petersen, T., & Vascon, S. (2025). A gradient-boosted tree framework to model the ice thickness of the world's glaciers (IceBoost v1.1). *Geoscientific Model Development*, *18*(9), 2545–2568. https://doi.org/10.5194/gmd-18-2545-2025

Merdith, A. S., Williams, S. E., Collins, A. S., Tetley, M. G., Mulder, J. A., Blades, M. L., et al. (2021). Extending full-plate tectonic models into deep time: Linking the Neoproterozoic and the Phanerozoic. *Earth-Science Reviews*, *214*, 103477. https://doi.org/10.1016/j.earscirev.2020.103477

Morlighem, M., Rignot, E., Seroussi, H., Larour, E., Ben Dhia, H., & Aubry, D. (2011). A mass conservation approach for mapping glacier ice thickness. *Geophysical Research Letters*, *38*(19). https://doi.org/10.1029/2011GL048659

Morlighem, M., Williams, C. N., Rignot, E., An, L., Arndt, J. E., Bamber, J. L., et al. (2017). BedMachine v3: Complete Bed Topography and Ocean Bathymetry Mapping of Greenland From Multibeam Echo Sounding Combined With Mass Conservation. *Geophysical Research Letters*, *44*(21), 11,051-11,061. https://doi.org/10.1002/2017GL074954

Morlighem, M., Williams, C., Rignot, E., An, L., Arndt, J. E., Bamber, J., et al. (2025). IceBridge BedMachine Greenland, Version 6 [Data set]. NASA National Snow and Ice Data Center Distributed Active Archive Center. https://doi.org/10.5067/6B6B225B8V2D

Morlighem, M., Charrassin, R., Maffezzoli, N., Millan, R., Ockenden, H., Schlegel, N.-J., et al. (2026). New high-resolution subglacial bed topography and coastal bathymetry of the Antarctic and Greenland Ice Sheets, Philosophical Transactions of the Royal Society A: Mathematical, Physical and Engineering Sciences, 384, 20240538, https://doi.org/10.1098/rsta.2024.0538

Mouginot, J., Rignot, E., Bjørk, A. A., Broeke, M. van den, Millan, R., Morlighem, M., et al. (2019). Forty-six years of Greenland Ice Sheet mass balance from 1972 to 2018. *Proceedings of the National Academy of Sciences*, *116*(19), 9239–9244. https://doi.org/10.1073/pnas.1904242116

Mudd, S. M., Roda-Boluda, D., Goren, L., & Clubb, Fiona J. (2022). Beyond the Long Profile. In *Treatise on Geomorphology* (2nd ed., Vol. 6.1, pp. 22–52). Academic Press. https://doi.org/10.1016/B978-0-12-818234-5.00026-2

Ng, F. S. L., Ignéczi, Á., Sole, A. J., & Livingstone, S. J. (2018). Response of Surface Topography to Basal Variability Along Glacial Flowlines. *Journal of Geophysical Research: Earth Surface*, *123*(10), 2319–2340. https://doi.org/10.1029/2017JF004555

Ockenden, H., Bingham, R. G., Curtis, A., & Goldberg, D. (2022). Inverting ice surface elevation and velocity for bed topography and slipperiness beneath Thwaites Glacier. *The Cryosphere*, *16*(9), 3867–3887. https://doi.org/10.5194/tc-16-3867-2022

Ockenden, H., Bingham, R. G., Curtis, A., & Goldberg, D. (2023). Ice-flow perturbation analysis: a method to estimate ice-sheet bed topography and conditions from surface datasets. *Journal of Glaciology*, 1–10. https://doi.org/10.1017/jog.2023.50

Ockenden, H., Bingham, R. G., Goldberg, D., Curtis, A., & Morlighem, M. (2026). Complex mesoscale landscapes beneath Antarctica mapped from space. *Science*, *391*(6782), 314–319. https://doi.org/10.1126/science.ady2532

Paxman, G. J. G. (2023). Patterns of valley incision beneath the Greenland Ice Sheet revealed using automated mapping and classification. *Geomorphology*, *436*, 108778. https://doi.org/10.1016/j.geomorph.2023.108778

Paxman, G. J. G., Tinto, K. J., & Austermann, J. (2021). Neogene-Quaternary Uplift and Landscape Evolution in Northern Greenland Recorded by Subglacial Valley Morphology. *Journal of Geophysical Research: Earth Surface*, *126*(12), e2021JF006395. https://doi.org/10.1029/2021JF006395

Paxman, G. J. G., Austermann, J., & Hollyday, A. (2022). Total isostatic response to the complete unloading of the Greenland and Antarctic Ice Sheets. *Scientific Reports*, *12*(1), 11399. https://doi.org/10.1038/s41598-022-15440-y

Paxman, G. J. G., Jamieson, S. S. R., Dolan, A. M., & Bentley, M. J. (2024). Subglacial valleys preserved in the highlands of south and east Greenland record restricted ice extent during past warmer climates. *The Cryosphere*, *18*(3), 1467–1493. https://doi.org/10.5194/tc-18-1467-2024

Paxman, G. J. G., Austermann, J., & Hollyday, A. (2026). Grid files of the total isostatic response to the complete unloading of the Greenland and Antarctic Ice Sheets (version 3) (2026) [Data set]. Arctic Data Center. https://doi.org/10.18739/A22Z12R8C

Pritchard, H. D., Fretwell, P. T., Fremand, A. C., Bodart, J. A., Kirkham, J. D., Aitken, A., et al. (2025). Bedmap3 updated ice bed, surface and thickness gridded datasets for Antarctica. *Scientific Data*, *12*(1), 414. https://doi.org/10.1038/s41597-025-04672-y

Rasmussen, T. M., & Dawes, P. R. (2011). Kennedy Channel and its geophysical lineaments: new evidence that the Wegener Fault is a myth. *GEUS Bulletin*, *23*, 69–72. https://doi.org/10.34194/geusb.v23.4875

Robel, A. A., Sim, S. J., Meyer, C., Siegfried, M. R., & Gustafson, C. D. (2023). Contemporary ice sheet thinning drives subglacial groundwater exfiltration with potential feedbacks on glacier flow. *Science Advances*, *9*(33), eadh3693. https://doi.org/10.1126/sciadv.adh3693

Robin, G. D. Q., Evans, S., & Bailey, J. T. (1969). Interpretation of radio echo sounding in polar ice sheets. *Philosophical Transactions of the Royal Society of London. Series A, Mathematical and Physical Sciences*, *265*(1166), 437–505. https://doi.org/10.1098/rsta.1969.0063

Schwangart, W., & Scherler, D. (2014). TopoToolbox. Retrieved June 21, 2023, from https://www.mathworks.com/matlabcentral/fileexchange/50124-topotoolbox

Sergienko, O. V. (2012). The effects of transverse bed topography variations in ice-flow models. *Journal of Geophysical Research: Earth Surface*, *117*(F3). https://doi.org/10.1029/2011JF002203

Sergienko, O. V. (2013). Glaciological twins: basally controlled subglacial and supraglacial lakes. *Journal of Glaciology*, *59*(213), 3–8. https://doi.org/10.3189/2013JoG12J040

Sergienko, O. V., Creyts, T. T., & Hindmarsh, R. C. A. (2014). Similarity of organized patterns in driving and basal stresses of Antarctic and Greenland ice sheets beneath extensive areas of basal sliding. *Geophysical Research Letters*, *41*(11), 3925–3932. https://doi.org/10.1002/2014GL059976

Seybold, H., Rothman, D. H., & Kirchner, J. W. (2017). Climate's watermark in the geometry of stream networks. *Geophysical Research Letters*, *44*(5), 2272–2280. https://doi.org/10.1002/2016GL072089

Seybold, H., Kite, E., & Kirchner, J. W. (2018). Branching geometry of valley networks on Mars and Earth and its implications for early Martian climate. *Science Advances*, *4*(6), eaar6692. https://doi.org/10.1126/sciadv.aar6692

Srivastava, S. P., & Falconer, R. K. H. (1982). Nares Strait: a conflict between plate tectonic predictions and geological interpretation. *Meddelelser Om Grønland. Geoscience*, *8*, 339–352. https://doi.org/10.7146/moggeosci.v8i.139606

References from the Supporting Information

Canny, J. (1986). A Computational Approach to Edge Detection. *IEEE Transactions on Pattern Analysis and Machine Intelligence*, *PAMI-8*(6), 679–698. https://doi.org/10.1109/TPAMI.1986.4767851

Fitton, N. C., & Cox, S. J. D. (1998). Optimising the application of the Hough transform for automatic feature extraction from geoscientific images. *Computers & Geosciences*, *24*(10), 933–951. https://doi.org/10.1016/S0098-3004(98)00070-3

Kjær, K. H., Larsen, N. K., Binder, T., Bjørk, A. A., Eisen, O., Fahnestock, M. A., et al. (2018). A large impact crater beneath Hiawatha Glacier in northwest Greenland. *Science Advances*, *4*(11), eaar8173. https://doi.org/10.1126/sciadv.aar8173

MacGregor, J. A., Bottke, W. F., Fahnestock, M. A., Harbeck, J. P., Kjær, K. H., Paden, J. D., et al. (2019). A Possible Second Large Subglacial Impact Crater in Northwest Greenland. *Geophysical Research Letters*, *46*(3), 1496–1504. https://doi.org/10.1029/2018GL078126

Thorsteinsson, T., Raymond, C. F., Gudmundsson, G. H., Bindschadler, R. A., Vornberger, P., & Joughin, I. (2003). Bed topography and lubrication inferred from surface measurements on fast-flowing ice streams. *Journal of Glaciology*, *49*(167), 481–490. https://doi.org/10.3189/172756503781830502

Wang, J., & Howarth, P. J. (1990). Use of the Hough transform in automated lineament. *IEEE Transactions on Geoscience and Remote Sensing*, *28*(4), 561–567. https://doi.org/10.1109/TGRS.1990.572949